

Coupling Load-Following Control with OPF

Mohammadhafez Bazrafshan, *Student Member, IEEE*,

Nikolaos Gatsis, *Member, IEEE*, Ahmad F. Taha, *Member, IEEE*, Joshua A. Taylor, *Member, IEEE*

Abstract—In this paper, the optimal power flow (OPF) problem is augmented to account for the costs associated with the load-following control of a power network. Load-following control costs are expressed through the linear quadratic regulator (LQR). The power network is described by a set of nonlinear differential algebraic equations (DAEs). By linearizing the DAEs around a known equilibrium, a linearized OPF that accounts for steady-state operational constraints is formulated first. This linearized OPF is then augmented by a set of linear matrix inequalities that are algebraically equivalent to the implementation of an LQR controller. The resulting formulation, termed LQR-OPF, is a semidefinite program which furnishes optimal steady-state setpoints and an optimal feedback law to steer the system to the new steady state with minimum load-following control costs. Numerical tests demonstrate that the setpoints computed by LQR-OPF result in lower overall costs and frequency deviations compared to the setpoints of a scheme where OPF and load-following control are considered separately.

Index Terms—Optimal power flow, load-following control, linear quadratic regulator, semidefinite programming.

I. INTRODUCTION

CAPACITY expansion and generation planning, economic dispatch, frequency regulation, and automatic generation control (AGC) are decision making problems in power networks that are solved over different time horizons. These problems range from decades in planning to several seconds in transient control. Although decisions made in shorter time periods may negatively affect performance over longer time periods, these problems have traditionally been treated separately. For example, optimization is used for optimal power flow (OPF) and economic dispatch while feedback control theory is used for frequency regulation.

This paper aims to integrate two crucial power network problems with different time-scales. The first problem is the steady-state OPF, whose decisions are updated every few minutes (e.g., 5 minutes for real-time market balancing). The second is the problem of load-following control that spans the time-scale of several seconds to one minute. Load-following control, also known as secondary frequency control [1], is responsible for maintaining system frequencies at nominal values during normal load fluctuations [2].

For a forecasted load level, optimal steady-state setpoints that also minimize costs of load-following control are sought. Steady-state costs account for generator power outputs. Control costs account for the action required to drive the deviation of frequency and voltage signals from their optimal OPF setpoints to zero via the linear quadratic regulator (LQR). The proposed formulation also provides, as an output, a feedback law to guide the system dynamics to optimal OPF setpoints.

This material is based upon work supported by the National Science Foundation Grants ECCS-1462404 and CCF-1421583.

A. Literature Review

Recent research efforts, organized below in two categories, have showcased the economic and technical merits of jointly tackling steady-state and control problems in power networks.

The first category focuses on frequency regulation with a view towards the economic dispatch [3]–[10]. These works design controllers based on feedback from frequency measurements and guarantee the stability of system dynamics—characterized by the swing equation—while ensuring that system states converge to steady-state values optimal for some form of the economic dispatch problem.

The designs of these feedback control laws may come from averaging-based controllers as in [3]–[5]. By leveraging a continuous-time version of a dual algorithm, generalized versions of the aforementioned controllers are developed in [6], including the classical AGC as a special case. Similar control designs come from interpretation of network dynamics as iterations of a primal-dual algorithm that solves an OPF. For example, [7] introduces a primary frequency control that minimizes a reverse-engineered load disutility function, and [8] introduces a modified AGC that solves an economic dispatch with limited operational constraints.

A frequency control law that further solves economic dispatch with nonlinear power flows in tree networks is devised in [9] by borrowing virtual dynamics from the KKT conditions. A novel method to tackle a load-side control problem including linear equality or inequality constraints for arbitrary network topologies is presented in [10]. The chief attractive feature of [3]–[10] is that they afford decentralized or distributed implementations. Moreover, works such as [6] and [9] develop controllers accounting for nonlinear power flow equations.

The second category focuses on OPF variations with enhanced stability measures. The goal is to obtain optimal steady-state setpoints less vulnerable to disturbances, rather than seeking a stabilizing control law. This goal is achieved by incorporating additional constraints in OPF that account for the stability of the steady-state optimal point.

In the context of transient stability, a classical reference is [11] where system differential equations are converted to algebraic ones and added to the OPF. More recently, trajectory sensitivity analysis has been extensively used to accommodate transient stability specifications in the form of linear constraints within the OPF. Typically, these constraints are based on stability margins obtained from the (extended) equal-area criterion [12]–[15]. In particular, [12] augments the OPF with automated computationally-efficient rotor angle constraints around a base stable trajectory. Transient-stability constrained OPF formulations that are robust to uncertainty in load dynamics and wind power generation have also been

developed [13], [14]. Load-shedding minimization has been pursued in [15], where in addition to angle stability margins, trajectory sensitivities have been used to approximate constraints on voltage and frequency security margins.

In the realm of small-signal stability, distance from rotor instability is guaranteed in [16] by providing a set of stressed load conditions as a supplement to OPF. The spectral abscissa, that is, the largest real part of system state matrix eigenvalues, is upper bounded by a negative number in [17], yielding a non-smooth OPF. A simpler optimization problem is pursued in [18] using the pseudo-spectral abscissa as stability measure. Based on Lyapunov's stability theorem and the system state matrix, [19] incorporates small-signal stability constraints into the OPF. Since the state matrix is a function of the steady-state variables, the overall formulation becomes a nonlinear and nonconvex semidefinite program (SDP).

B. Paper contributions and organization

The paper contributions are as follows:

- An OPF framework is proposed that solves for optimal steady-state setpoints and also provides an optimal load-following control law to drive the system to those setpoints. Optimality of the control law is appraised by an integral cost on time-varying deviation of system states and controls from their optimal setpoints. An LQR controller is then applied which minimizes this cost by providing a feedback law that is a linear combination of system state deviations. LQR has previously been used in the context of megawatt-frequency control [20] and control of oscillatory dynamics [21]. The proposed framework, in distinction, accounts for LQR costs from within the steady-state time-scale.
- The setpoints computed by the proposed formulation, termed LQR-OPF, result in lower overall costs and frequency fluctuations compared to the setpoints of a scheme where OPF and load-following control are decoupled. The proposed framework also allows time-varying control costs to be dependent on steady-state variables. This dependence enables subsequent regulation pricing schemes similar to [22] where for example, the cost of frequency regulation is made dependent on steady-state power generation.
- In comparison to [3]–[10], the formulation in this paper includes voltage dynamics, reactive powers, AC power flows, and a more realistic dynamical model of the synchronous generator that distinguishes between generator internal and external quantities. Costs incurred due to deviations of system states and controls from their optimal setpoints are also accounted for. In relation to [11]–[19], the proposed approach incorporates load-following control constraints into the OPF; but as an extra output, the required control law to steer the system to stability is also provided.
- The effectiveness of the derived control law is demonstrated via numerical simulations on the power system described by *nonlinear differential-algebraic equations* (DAEs). We further exhibit that the steady-state setpoints provided by the proposed LQR-OPF yield smaller overall system costs even when the traditional AGC is used for load following.

In this paper, in order to obtain a stabilizing feedback law, nonlinear DAEs are linearized around a known equilibrium

point with respect to the system states and algebraic variables. It should be emphasized that this linearization is different than that of trajectory sensitivity analysis. In the latter, the system dynamics are linearized around a known trajectory with respect to system initial conditions and parameters [23], [24]. Formulations in [12]–[14] that use trajectory sensitivity analysis are suitable for transient stability where it is required to limit generators' angle separation subject to contingencies and large disturbances, e.g., line trips due to three-phase faults. On the other hand, the load-following or secondary control, which is considered in this paper, aims at maintaining frequencies at their nominal value during normal load changes.

The paper is organized as follows. The power system model is laid out in Section II, followed by a description of a generalized OPF. System linearization is pursued in Section III. The proposed formulation coupling OPF and load-following control is detailed in Section IV. Specific generator models, power flow equations, and connections to the standard OPF are provided in Section VI. Section VII numerically verifies the merits of the proposed method. Section VIII provides pointers for integrating more power system applications into our proposed framework as future work.

II. POWER SYSTEM MODEL

Consider a power network with N buses where $\mathcal{N} := \{1, \dots, N\}$ is the set of nodes. Define the partition $\mathcal{N} = \mathcal{G} \cup \mathcal{L}$ where $\mathcal{G} = \{1, \dots, G\}$ collects G buses that contain generators (and possibly also loads) and $\mathcal{L} = \{G + 1, \dots, G + L\}$ collects the remaining L load-only buses. Notice that $N = G + L$. For a generator $i \in \mathcal{G}$ with n_s states and n_c control inputs, denote by $\mathbf{x}_i(t) \in \mathbb{R}^{n_s}$ the time-varying vector of state variables, and denote by $\mathbf{u}_i(t) \in \mathbb{R}^{n_c}$ the time-varying control inputs. For example, adopting a fourth-order model yields $n_s = 4$ and $n_c = 2$ with $\mathbf{x}_i(t) = \{\delta_i(t), \omega_i(t), e_i(t), m_i(t)\}$ and $\mathbf{u}_i(t) = \{r_i(t), f_i(t)\}$ where $\delta_i(t)$, $\omega_i(t)$, $e_i(t)$, $m_i(t)$, $r_i(t)$, and $f_i(t)$ respectively denote the generator internal phase angle, rotor electrical velocity, internal EMF, mechanical power input, reference power setting, and internal field voltage. Further details are given in Section VI-A.

Denote by $\mathbf{a}_i(t)$ the vector of algebraic variables. For load nodes $i \in \mathcal{L}$, $\mathbf{a}_i(t) = \{v_i(t), \theta_i(t)\}$, where $v_i(t)$ and $\theta_i(t)$ denote the terminal load voltage and phase angle. For generator nodes $i \in \mathcal{G}$, $\mathbf{a}_i(t) = \{p_{g_i}(t), q_{g_i}(t), v_i(t), \theta_i(t)\}$, where $p_{g_i}(t)$, $q_{g_i}(t)$, $v_i(t)$, and $\theta_i(t)$ respectively denote generator real and reactive power, terminal voltage and phase angle. For brevity, the dependency of variables \mathbf{x}_i , \mathbf{a}_i , and \mathbf{u}_i on t is dropped, and the notations $\mathbf{x} := \{\mathbf{x}_i\}_{i \in \mathcal{G}} \in \mathbb{R}^{n_s G}$, $\mathbf{u} := \{\mathbf{u}_i\}_{i \in \mathcal{G}} \in \mathbb{R}^{n_c G}$, and $\mathbf{a} := \{\mathbf{a}_i\}_{i \in \mathcal{N}} \in \mathbb{R}^{2N+2G}$ are introduced. Finally, let $\mathbf{z} = \{\mathbf{x}, \mathbf{a}, \mathbf{u}\} \in \mathbb{R}^{(n_s+n_c+2)G+2N}$. The dynamics of a power system can be captured by a set of nonlinear DAEs

$$\dot{\mathbf{x}} = \mathbf{g}(\mathbf{x}, \mathbf{a}, \mathbf{u}), \quad (1a)$$

$$\mathbf{d} = \mathbf{h}(\mathbf{x}, \mathbf{a}), \quad (1b)$$

where $\mathbf{g} : \mathbb{R}^{(n_s+n_c+2)G+2N} \rightarrow \mathbb{R}^{n_s G}$ is given by adopting an appropriate dynamical model of the generator, and $\mathbf{h} : \mathbb{R}^{(n_s+2)G+2N} \rightarrow \mathbb{R}^{2G+2N}$ includes generator algebraic

equations as well as the network power flow equations. Vector \mathbf{d} collects all the network loads as well as leading zero entries coming from two generator algebraic equations per generator. A particular example of the mapping \mathbf{g} is provided in Section VI-A; for the corresponding form of the mapping \mathbf{h} and the vector \mathbf{d} see Section VI-B.

Given steady-state load conditions \mathbf{d}^{eq} , the system steady-state operating point is represented by an equilibrium of the DAEs (1). By setting $\dot{\mathbf{x}} = \mathbf{0}$ and allowing \mathbf{x} , \mathbf{a} , and \mathbf{u} to reach steady states \mathbf{x}^{eq} , \mathbf{a}^{eq} , and \mathbf{u}^{eq} , a system of $(n_s + 2)G + 2N$ algebraic equations in $(n_s + n_c + 2)G + 2N$ variables is derived:

$$\mathbf{0} = \mathbf{g}(\mathbf{x}^{\text{eq}}, \mathbf{a}^{\text{eq}}, \mathbf{u}^{\text{eq}}), \quad (2a)$$

$$\mathbf{d}^{\text{eq}} = \mathbf{h}(\mathbf{x}^{\text{eq}}, \mathbf{a}^{\text{eq}}). \quad (2b)$$

Let $\mathcal{F}(\mathbf{d}^{\text{eq}})$ denote the set of solutions to (2), where the dependency on the load conditions is made explicit. Suppose now that \mathbf{x}^{eq} , \mathbf{a}^{eq} , \mathbf{u}^{eq} are to be jointly optimized so that a certain objective function $c(\mathbf{x}^{\text{eq}}, \mathbf{a}^{\text{eq}}, \mathbf{u}^{\text{eq}})$ is minimized. This leads to a generalized OPF [for clarity, the notation $(\mathbf{x}^s, \mathbf{a}^s, \mathbf{u}^s)$ is used to denote optimization variables, and $(\mathbf{x}^{\text{eq}}, \mathbf{a}^{\text{eq}}, \mathbf{u}^{\text{eq}})$ is used to generically denote a DAE equilibrium].

$$\min_{\mathbf{x}^s, \mathbf{a}^s, \mathbf{u}^s} c(\mathbf{x}^s, \mathbf{a}^s, \mathbf{u}^s) \quad (3a)$$

$$\text{subj. to } \mathbf{0} = \mathbf{g}(\mathbf{x}^s, \mathbf{a}^s, \mathbf{u}^s), \quad (3b)$$

$$\mathbf{d}^s = \mathbf{h}(\mathbf{x}^s, \mathbf{a}^s), \quad (3c)$$

$$\mathbf{a}^s \in \mathcal{A}, \quad (3d)$$

where (3d) are the algebraic variable constraints on voltage magnitudes, line flow limits, and line current capacities. Note that the parameter vector \mathbf{d}^s (which includes the constant-power loads) is the input to (3). The term *generalized* refers to the fact that (3) considers models of generators within the OPF, see e.g., [25] for a recent OPF example with machine models. The connection between (3) and the standard OPF is explained in Section VI-C. The OPF problem (3) guarantees optimal steady-state operating costs, but does not provide minimal control costs. Prior to introducing a formulation that bridges stability with OPF, linear approximation of the system dynamics is required which is presented in the next section.

III. LINEAR APPROXIMATION OF SYSTEM DYNAMICS

To obtain an approximate dynamic, (1) is linearized around a known operating point $\mathbf{z}^0 := (\mathbf{x}^0, \mathbf{a}^0, \mathbf{u}^0) \in \mathcal{F}(\mathbf{d}^0)$. For example, the point \mathbf{z}^0 can be a solution of the load-flow corresponding to an operating point known to the system operator. The motivation behind this selection is to obtain tractable constraints to augment (3) as it allows the stability constraints to take the form of properly formulated linear matrix inequalities (LMIs). The derived control law is eventually applied to the nonlinear DAEs (1), rather than the linearization derived in this section.

Consider a generic *equilibrium* point $\mathbf{z}^0 \in \mathcal{F}(\mathbf{d}^0)$, where \mathbf{d}^0 is a known load vector. That is, the following holds:

$$\mathbf{0} = \mathbf{g}(\mathbf{x}^0, \mathbf{a}^0, \mathbf{u}^0), \quad (4a)$$

$$\mathbf{d}^0 = \mathbf{h}(\mathbf{x}^0, \mathbf{a}^0). \quad (4b)$$

Define $\Delta \mathbf{d}^s := \mathbf{d}^s - \mathbf{d}^0$ as the step-change difference between \mathbf{d}^s , the load for which the generalized OPF (3) is to be solved, and \mathbf{d}^0 , the generic load that will be used for linearization. Equations (1a) and (1b) can be linearized around $(\mathbf{x}^0, \mathbf{a}^0, \mathbf{u}^0)$ by setting $(\mathbf{x}, \mathbf{a}, \mathbf{u}) = (\mathbf{x}^0, \mathbf{a}^0, \mathbf{u}^0) + (\Delta \mathbf{x}, \Delta \mathbf{a}, \Delta \mathbf{u})$:

$$\Delta \dot{\mathbf{x}} = \mathbf{g}_x(\mathbf{z}^0) \Delta \mathbf{x} + \mathbf{g}_a(\mathbf{z}^0) \Delta \mathbf{a} + \mathbf{g}_u(\mathbf{z}^0) \Delta \mathbf{u}, \quad (5a)$$

$$\Delta \mathbf{d}^s = \mathbf{h}_x(\mathbf{x}^0, \mathbf{a}^0) \Delta \mathbf{x} + \mathbf{h}_a(\mathbf{x}^0, \mathbf{a}^0) \Delta \mathbf{a}, \quad (5b)$$

where the notation \mathbf{g}_x defines the Jacobian with respect to \mathbf{x} , and \mathbf{g}_a , \mathbf{g}_u , \mathbf{h}_x , and \mathbf{h}_a are similarly defined. It is also understood that $\Delta \mathbf{x}$, $\Delta \mathbf{a}$, $\Delta \mathbf{u}$ are functions of time.

Equation (5) represents a set of linear DAEs. Next, (5) is leveraged in order to develop a proper linear dynamical system that represents the network without algebraic constraints. In particular, assuming invertibility of $\mathbf{h}_a(\mathbf{x}^0, \mathbf{a}^0)$, (5b) can be solved for the algebraic variables as

$$\Delta \mathbf{a} = -\mathbf{h}_a^{-1}(\mathbf{x}^0, \mathbf{a}^0) (-\Delta \mathbf{d}^s + \mathbf{h}_x(\mathbf{x}^0, \mathbf{a}^0) \Delta \mathbf{x}). \quad (6)$$

The assumption on invertibility of $\mathbf{h}_a(\mathbf{x}^0, \mathbf{a}^0)$ is very mild in the sense that it holds for practical networks and for various operating points; see also [18] and references therein for sufficient conditions in a similar construction. Then, substituting (6) in (5a) yields

$$\Delta \dot{\mathbf{x}} = \mathbf{A}(\mathbf{z}^0) \Delta \mathbf{x} + \mathbf{B}(\mathbf{z}^0) \Delta \mathbf{u} + \mathbf{g}_a(\mathbf{z}^0) \mathbf{h}_a^{-1}(\mathbf{x}^0, \mathbf{a}^0) \Delta \mathbf{d}^s, \quad (7)$$

where $\mathbf{A}(\mathbf{z}^0) = \mathbf{g}_x(\mathbf{z}^0) - \mathbf{g}_a(\mathbf{z}^0) \mathbf{h}_a^{-1}(\mathbf{x}^0, \mathbf{a}^0) \mathbf{h}_x(\mathbf{x}^0, \mathbf{a}^0)$, and $\mathbf{B}(\mathbf{z}^0) = \mathbf{g}_u(\mathbf{z}^0)$.

IV. COUPLING LOAD-FOLLOWING CONTROL WITH OPF

In this section, an optimal control problem using the LQR is presented to stabilize the linear dynamical system (7) to an equilibrium point, while ensuring minimal steady-state operating costs for the equilibrium of the linearized dynamics. The equilibrium of the linearized dynamics is denoted by $\mathbf{z}^s = (\mathbf{x}^s, \mathbf{a}^s, \mathbf{u}^s)$ to distinguish it from the equilibrium of the true nonlinear system in e.g., (2). Section IV-A leverages the linearized dynamical system (7) to obtain a *linear approximation* of the constraints (3b) and (3c)—this yields a linearized OPF. The objective of Section IV-B is to incorporate stability measures with respect to the dynamical system (7) in the linearized OPF. The resulting formulation outputs optimal steady-state values $\mathbf{z}^s = (\mathbf{x}^s, \mathbf{a}^s, \mathbf{u}^s)$ together with the optimal control law that drives the dynamic variables to stability.

A. Linear approximation of the generalized OPF

The steady state of (5) obtained by setting $\Delta \dot{\mathbf{x}} = \mathbf{0}$ yields the following system:

$$\mathbf{0} = [\mathbf{g}_x(\mathbf{z}^0), \mathbf{g}_a(\mathbf{z}^0), \mathbf{g}_u(\mathbf{z}^0)] (\mathbf{z}^s - \mathbf{z}^0), \quad (8a)$$

$$\Delta \mathbf{d}^s = [\mathbf{h}_x(\mathbf{x}^0, \mathbf{a}^0), \mathbf{h}_a(\mathbf{x}^0, \mathbf{a}^0)] ((\mathbf{x}^s, \mathbf{a}^s) - (\mathbf{x}^0, \mathbf{a}^0)) \quad (8b)$$

The equations in (8) are therefore a linear approximation of constraints (3b) and (3c), which leads to a linearized version of OPF, formulated as follows:

Linearized OPF :

$$\min_{\mathbf{x}^s, \mathbf{a}^s, \mathbf{u}^s} c(\mathbf{x}^s, \mathbf{a}^s, \mathbf{u}^s) \text{ subj. to (8) and } \mathbf{a}^s \in \mathcal{A}. \quad (9)$$

Notice that (9) has the linearized version of power flow equations as part of its constraint set.

B. LQR-OPF formulation

The previous section derived (9), which is the linear approximation of the generalized OPF (3). Likewise, the linear system in (7) is the linear approximation of the system dynamics (1a) and (1b) around \mathbf{z}^0 . This section augments the linearized OPF (9) with optimal control of the dynamical system in (7).

Writing (7) at its equilibrium \mathbf{z}^s , that is, setting $\Delta\dot{\mathbf{x}} = \mathbf{0}$, $\Delta\mathbf{x} = \Delta\mathbf{x}^s$, and $\Delta\mathbf{u} = \Delta\mathbf{u}^s$, yields

$$\mathbf{0} = \mathbf{A}(\mathbf{z}^0)\Delta\mathbf{x}^s + \mathbf{B}(\mathbf{z}^0)\Delta\mathbf{u}^s + \mathbf{g}_a(\mathbf{z}^0)\mathbf{h}_a(\mathbf{x}^0, \mathbf{a}^0)^{-1}\Delta\mathbf{d}^s. \quad (10)$$

Subtracting (10) from (7) yields the following system with the new state variable $\Delta\mathbf{x}' := \Delta\mathbf{x} - \Delta\mathbf{x}^s$ and new control variable $\Delta\mathbf{u}' = \Delta\mathbf{u} - \Delta\mathbf{u}^s$:

$$\Delta\dot{\mathbf{x}}' = \mathbf{A}(\mathbf{z}^0)\Delta\mathbf{x}' + \mathbf{B}(\mathbf{z}^0)\Delta\mathbf{u}'. \quad (11)$$

The initial conditions of (11) are $\Delta\mathbf{x}'(0) = \Delta\mathbf{x}(0) - \Delta\mathbf{x}^s = \mathbf{x}(0) - \mathbf{x}^s$. When $\Delta\mathbf{x}$ in (5) or (7) converges to $\Delta\mathbf{x}^s$, $\Delta\mathbf{x}'$ in (11) converges to $\mathbf{0}$. The objective is to penalize the control effort to drive $\Delta\mathbf{x}'$ to $\mathbf{0}$.

To this end, weights on the control actions and state deviations are considered. In particular, an optimal LQR controller to drive the system states $\Delta\mathbf{x}'$ through a state-feedback control $\Delta\mathbf{u}'$ to their zero steady-state values is considered. By augmenting the linearized OPF in (9), this LQR-based OPF is written as follows:

$$\min_{\substack{\mathbf{z}^s = \{\mathbf{x}^s, \mathbf{a}^s, \mathbf{u}^s\} \\ \Delta\mathbf{x}', \Delta\mathbf{u}'}} c(\mathbf{z}^s) + \frac{T_{\text{lqr}}}{2} \int_0^{t_f} \Delta\mathbf{x}'^\top \mathbf{Q} \Delta\mathbf{x}' + \Delta\mathbf{u}'^\top \mathbf{R} \Delta\mathbf{u}' dt \quad (12a)$$

$$\text{subj. to } \Delta\dot{\mathbf{x}}' = \mathbf{A}(\mathbf{z}^0)\Delta\mathbf{x}' + \mathbf{B}(\mathbf{z}^0)\Delta\mathbf{u}' \quad (12b)$$

$$\Delta\mathbf{x}'(0) = \mathbf{x}(0) - \mathbf{x}^s \quad (12c)$$

$$(8a), (8b), \mathbf{a}^s \in \mathcal{A}, \quad (12d)$$

where \mathbf{Q} and \mathbf{R} are positive definite matrices penalizing state and control actions deviations; T_{lqr} is a scaling factor to compensate for the time-scale of the stability control problem; t_f is the optimization time-scale for the OPF problem which is typically in minutes. Since t_f is in minutes, the finite horizon LQR problem can be replaced with an infinite horizon LQR formulation (i.e., $t_f = \infty$) as the solution to the Riccati equation reaches steady state [26]. In (12c), if the system is assumed to operate at \mathbf{x}^0 , then $\Delta\mathbf{x}(0) = \mathbf{0}$, yielding $\Delta\mathbf{x}'(0) = \mathbf{x}^0 - \mathbf{x}^s$.

Regulating state and control actions can be dependent on the operating points to encourage smaller steady-state variations. For example, regulating a generator's frequency becomes more costly as the real power generation increases [22]. This coupling is captured by considering \mathbf{Q}^{-1} and \mathbf{R}^{-1} to be affine functions of steady-state variable \mathbf{z}^s . In particular, assume \mathbf{Q}^{-1} and \mathbf{R}^{-1} to be diagonal matrices as follows

$$\mathbf{Q}(\mathbf{z}^s)^{-1} = \mathbf{Q}_0^{-1} + \mathbf{Q}_1^{-1}\text{diag}(\mathbf{a}^s), \quad (13a)$$

$$\mathbf{R}(\mathbf{z}^s)^{-1} = \mathbf{R}_0^{-1} + \mathbf{R}_1^{-1}\text{diag}(\mathbf{a}^s). \quad (13b)$$

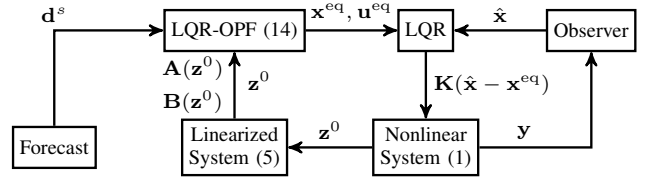


Fig. 1. Overall design of the proposed method. The LQR-OPF uses the forecast information to determine the optimal setpoints for the system. The feedback control law generated by the LQR drives the system to the optimal steady-state with minimized control costs.

Matrices \mathbf{Q}_0 , \mathbf{Q}_1 , \mathbf{R}_0 , and \mathbf{R}_1 are selected so that $\mathbf{Q}(\mathbf{z}^s)$ and $\mathbf{R}(\mathbf{z}^s)$ are positive definite over the bounded range of \mathbf{a}^s prescribed by the set \mathcal{A} .

The corresponding infinite horizon LQR augmenting the linearized OPF (12) can be written as an SDP, as follows:

LQR-OPF:

$$\min_{\mathbf{S}, \mathbf{z}^s = \{\mathbf{x}^s, \mathbf{a}^s, \mathbf{u}^s\}} c(\mathbf{z}^s) + \frac{T_{\text{lqr}}}{2} \gamma \quad (14a)$$

$$\text{subj. to } (8a), (8b), \mathbf{a}^s \in \mathcal{A} \quad (14b)$$

$$\begin{bmatrix} -\gamma & (\mathbf{x}^s - \mathbf{x}^0)^\top \\ \mathbf{x}^s - \mathbf{x}^0 & -\mathbf{S} \end{bmatrix} \preceq \mathbf{O} \quad (14c)$$

$$\begin{bmatrix} \mathbf{A}^\top \mathbf{S} + \mathbf{S} \mathbf{A} & & & \\ + \mathbf{B} \mathbf{Y} + \mathbf{Y}^\top \mathbf{B}^\top & \mathbf{S} & & \mathbf{Y}^\top \\ \mathbf{S} & -\mathbf{Q}^{-1}(\mathbf{z}^s) & & \mathbf{O} \\ \mathbf{Y} & \mathbf{O} & & -\mathbf{R}^{-1}(\mathbf{z}^s) \end{bmatrix} \preceq \mathbf{O} \quad (14d)$$

$$\mathbf{S} \succeq \mathbf{O}. \quad (14e)$$

The optimal control law generated from the optimal control problem (12) is $\Delta\mathbf{u}' = \mathbf{K}\Delta\mathbf{x}'$ where $\mathbf{K} = -\mathbf{R}^{-1}(\mathbf{z}^s)\mathbf{B}(\mathbf{z}^0)^\top \mathbf{S}^{*-1}$ is the optimal state feedback control gain and $(\mathbf{S}^*, \mathbf{z}^s)$ is an optimizer of (14). The reader is referred to [26] for the derivation of this control law.

The LQR-OPF problem (14) is an SDP which solves jointly for the new steady-state variables \mathbf{z}^s and the matrix \mathbf{S} while guaranteeing the stability of the linearized system in (7). The two problems of OPF and stability control are coupled in (14) through the LQR weight matrices—with \mathbf{Q}^{-1} and \mathbf{R}^{-1} being affine functions—as well as through the term $\mathbf{x}^s - \mathbf{x}^0$ in LMI (14c). It is worth noting that γ in (14) is equal to the integral in the objective of (12) with $t_f = \infty$.

The optimal steady-state solution \mathbf{z}^s of the LQR-OPF problem (14) satisfies the linearized steady-state equations (8). In order to obtain an equilibrium for the true nonlinear DAEs (2), generator setpoints from \mathbf{z}^s are extracted as follows. For generator $i \in \mathcal{G}$, set $v_i^{\text{eq}} = v_i^s$. If i is nonslack, set $p_{g_i}^{\text{eq}} = p_{g_i}^s$. If i is slack, set $\theta_i^{\text{eq}} = \theta_i^s$. Then, the system of equations (2) is solved to obtain an equilibrium \mathbf{z}^{eq} for the nonlinear DAEs in (1). This task essentially amounts to solving two separate sets of nonlinear equalities: first a standard load-flow is solved to obtain the remainder of algebraic variables $q_{g_i}^{\text{eq}}$ for $i \in \mathcal{G}$, v_i^{eq} for $i \in \mathcal{L}$, $p_{g_i}^{\text{eq}}$ if i is slack, and θ_i^{eq} for i nonslack. Second, by incorporating the algebraic variables in generator equations, the equilibrium states and controls of the generators, that is \mathbf{x}^{eq} and \mathbf{u}^{eq} , are obtained. This process is detailed in Section VII that includes simulations.

Figure 1 demonstrates the overall design and the integration of the proposed LQR-OPF into the power system operation. Initially, the system is operating at a known equilibrium point \mathbf{z}^0 . Using this known operating point, the state-space matrices $\mathbf{A}(\mathbf{z}^0)$ and $\mathbf{B}(\mathbf{z}^0)$ are computed according to (7). This information is then provided to the LQR-OPF block together with a forecast \mathbf{d}^s of the demand at the next steady state. The LQR-OPF calculates the optimal generator control setpoints included in \mathbf{u}^{eq} as well as the optimal state setpoints for the next steady state \mathbf{x}^{eq} . Upon providing the LQR block with optimal setpoints \mathbf{x}^{eq} and \mathbf{u}^{eq} , the LQR control law $\mathbf{K}(\mathbf{x} - \mathbf{x}^{\text{eq}}) + \mathbf{u}^{\text{eq}}$ is then applied to the nonlinear power system and drives the system to the new desired optimal point \mathbf{z}^{eq} .

The purpose of LQR-OPF (14) is to generate *steady-state operating points* with desirable stability properties and minimal secondary control effort, so that the optimal \mathbf{z}^{eq} in (14) is cognizant of dynamic stability constraints. The proposed LQR-OPF facilitates the development of a more general framework where various dynamical system applications can be integrated with static operational constraints, leading to the computation of stability-aware operating points—more concrete pointers to this end are provided in Section VIII.

Remark 1. In the previous sections, availability of the full state-vector $\mathbf{x}(t)$ (i.e., angles, frequencies, and EMFs for generators) is assumed for the optimal control law $\mathbf{u}(t)$. This assumption entails that sensors such as phasor measurement units (PMU) generate $\mathbf{x}(t)$ for all generator buses in the network. However, a PMU is not needed on all generator buses, as dynamic state estimation tools for power networks can be leveraged. See e.g., [27], [28] for estimation through Kalman filters and [29] for deterministic observers. For example, it has been previously demonstrated in [29] that 12 PMUs are sufficient to estimate the 10th order dynamics of the 16 generators in the New England 68-bus power network.

Remark 2. Problem (14) can be straightforwardly extended to include convex relaxations of the nonlinear power flow equations (such as SDP relaxations [30]) in place of the linearized power flow constraints (8a) and (8b).

V. APPROXIMATE SOLVER FOR THE LQR-OPF

The LQR-OPF problem presented in (14) has two LMIs and may be computationally expensive to solve for very large networks via interior-point methods. In this section, an algorithm to approximately solve (14) is developed.

To this end, consider the following nonconvex optimization:

$$\min_{\mathbf{z}^s = \{\mathbf{x}^s, \mathbf{a}^s, \mathbf{u}^s\}} c(\mathbf{a}^s) + \frac{T_{\text{lqr}}}{2} (\mathbf{x}^s - \mathbf{x}^0)^\top \mathbf{P} (\mathbf{x}^s - \mathbf{x}^0) \quad (15a)$$

$$\text{subj. to (8a), (8b), } \mathbf{a}^s \in \mathcal{A} \quad (15b)$$

$$\mathbf{A}^\top \mathbf{P} + \mathbf{P} \mathbf{A} - \mathbf{P} \mathbf{B} \mathbf{R}^{-1} (\mathbf{z}^s) \mathbf{B}^\top \mathbf{P} + \mathbf{Q}(\mathbf{z}^s) = \mathbf{O}, \quad (15c)$$

where (15c) is the well-known continuous algebraic Riccati equation (CARE). Problem (15) acts as a surrogate for (14) because the optimal values of problems (14) and (15) are equal. To see this, note first that the objective $c(\mathbf{a}^s)$ and constraints (8a), (8b), and $\mathbf{a}^s \in \mathcal{A}$ are the same for both

Algorithm 1 Approximate solver for LQR-OPF (ALQR-OPF)

```

1: Initialize  $o^{\text{best}} \leftarrow +\infty$ 
2: Set  $\mathbf{P}^{(0)}$  to the solution of CARE (15c) for  $\mathbf{z}^s = \mathbf{z}^0$ 
3: for  $k = 1 : k^{\text{max}}$  do
4:   Set  $\mathbf{z}^{(k)} = \{\mathbf{x}^{(k)}, \mathbf{a}^{(k)}, \mathbf{u}^{(k)}\}$  to the optimal solution
   of (15a)–(15b) for  $\mathbf{P} = \mathbf{P}^{(k-1)}$ 
5:   Set  $\mathbf{P}^{(k)}$  to the solution of CARE (15c) for  $\mathbf{z}^s = \mathbf{z}^{(k)}$ 
6:   if  $c(\mathbf{a}^{(k)}) + \frac{T_{\text{lqr}}}{2} (\mathbf{x}^{(k)} - \mathbf{x}^0)^\top \mathbf{P}^{(k)} (\mathbf{x}^{(k)} - \mathbf{x}^0) < o^{\text{best}}$ 
   then
7:      $o^{\text{best}} \leftarrow c(\mathbf{a}^{(k)}) + \frac{T_{\text{lqr}}}{2} (\mathbf{x}^{(k)} - \mathbf{x}^0)^\top \mathbf{P}^{(k)} (\mathbf{x}^{(k)} - \mathbf{x}^0)$ 
8:      $\mathbf{z}^s = \{\mathbf{x}^s, \mathbf{a}^s, \mathbf{u}^s\} \leftarrow \mathbf{z}^{(k)} = \{\mathbf{x}^{(k)}, \mathbf{a}^{(k)}, \mathbf{u}^{(k)}\}$ 
9:      $\mathbf{P}^* = \mathbf{P}^{(k)}$ 
10:   end if
11: end for

```

problems. Then, using the theory in [31, Sec. V], it can be shown that for any solution \mathbf{P} of the CARE in (15c), the quadratic form $(\mathbf{x}^s - \mathbf{x}^0)^\top \mathbf{P} (\mathbf{x}^s - \mathbf{x}^0)$ is equal to γ in (14a).

Although (15) is nonconvex, an efficient algorithm that alternates between variables \mathbf{z}^s and \mathbf{P} can be used to approximately solve (15). Specifically, with \mathbf{z}^s fixed, the CARE constraint (15c) can be solved for to obtain \mathbf{P} . Then, plugging \mathbf{P} into (15) and removing (15c) yields a quadratic program (QP), which can be efficiently solved. The process can be repeated as long as the objective in (15a) is improved, and is summarized in Algorithm 1. The algorithm is referred to as ALQR-OPF.

The technology for solving the CARE and QPs with very large number of variables has significantly matured and enables the efficient implementation of Algorithm 1. The numerical tests of Section VII indicate that Algorithm 1 does not practically compromise optimality and is scalable to networks with thousands of buses.

VI. GENERATOR MODEL, POWER FLOWS, AND OPF

The developments in this paper and the proposed LQR formulation are applicable to any generator dynamical model with control inputs. However, as an example, a specific form of mappings \mathbf{g} and \mathbf{h} is given in this section, which will be used for the numerical tests of Section VII.

A. Generator model

The fourth order model of the synchronous generator internal dynamics for node $i \in \mathcal{G}$ can be written as

$$\dot{\delta}_i = \omega_i - \omega_s \quad (16a)$$

$$\dot{\omega}_i = \frac{1}{M_i} [m_i - D_i(\omega_i - \omega_s) - p_{g_i}] \quad (16b)$$

$$\dot{e}_i = \frac{1}{\tau_{d_i}} \left[-\frac{x_{d_i}}{x'_{d_i}} e_i + \frac{x_{d_i} - x'_{d_i}}{x'_{d_i}} v_i \cos(\delta_i - \theta_i) + f_i \right] \quad (16c)$$

$$\dot{m}_i = \frac{1}{\tau_{c_i}} \left[r_i(t) - \frac{1}{R_i} (\omega_i - \omega_s) - m(t) \right] \quad (16d)$$

where M_i is the rotor's inertia constant (pu \times sec²), D_i is the damping coefficient (pu \times sec), τ_{d_i} is the direct-axis open-circuit time constant (sec), x_{d_i} and x_{q_i} are respectively the direct- and quadrature-axis synchronous reactances, and x'_{d_i} is the direct-axis transient reactance (pu). Equation (16d) is a

simplified model of a prime-mover generator with τ_{c_i} as the charging time (sec) and a speed-governing mechanism with R_i as the regulation constant ($\frac{\text{Rad} \times \text{Hz}}{\text{pu}}$). The mapping \mathbf{g} defined in (1a) is given by concatenating (16) for $i \in \mathcal{G}$.

The following algebraic equations relate the generator real and reactive power output with generator voltage, internal EMF, and internal angle and must hold at any time instant for generator nodes $i \in \mathcal{G}$:

$$0 = -p_{g_i} + \frac{e_i v_i}{x'_{di}} \sin(\delta_i - \theta_i) + \frac{x'_{di} - x_{qi}}{2x_{qi}x'_{di}} v_i^2 \sin[2(\delta_i - \theta_i)] \quad (17a)$$

$$0 = -q_{g_i} + \frac{e_i v_i}{x'_{di}} \cos(\delta_i - \theta_i) - \frac{x'_{di} + x_{qi}}{2x_{qi}x'_{di}} v_i^2 + \frac{x'_{di} - x_{qi}}{2x_{qi}x'_{di}} v_i^2 \cos[2(\delta_i - \theta_i)]. \quad (17b)$$

B. Power flow equations

Let $\mathbf{Y} = \mathcal{G} + j\mathcal{B}$ denote the network bus admittance matrix based on the π -model of transmission lines. Notice that \mathbf{Y} may include transformers, tap-changing voltage regulators, and phase shifters [32]. The power flow equations are

$$-p_{l_i} = -p_{g_i} + \mathcal{G}_{i,i} v_i^2 + \sum_{j \in \mathcal{N}_i} [\mathcal{G}_{i,j} v_i v_j \cos \theta_{ij} + \mathcal{B}_{i,j} v_i v_j \sin \theta_{ij}], i \in \mathcal{G}, \quad (18a)$$

$$-q_{l_i} = -q_{g_i} - \mathcal{B}_{i,i} v_i^2 + \sum_{j \in \mathcal{N}_i} [\mathcal{G}_{i,j} v_i v_j \sin \theta_{ij} - \mathcal{B}_{i,j} v_i v_j \cos \theta_{ij}], i \in \mathcal{G}, \quad (18b)$$

$$-p_{l_i} = \mathcal{G}_{i,i} v_i^2 + \sum_{j \in \mathcal{N}_i} [\mathcal{G}_{i,j} v_i v_j \cos \theta_{ij} + \mathcal{B}_{i,j} v_i v_j \sin \theta_{ij}], i \in \mathcal{L}, \quad (18c)$$

$$-q_{l_i} = -\mathcal{B}_{i,i} v_i^2 + \sum_{j \in \mathcal{N}_i} [\mathcal{G}_{i,j} v_i v_j \sin \theta_{ij} - \mathcal{B}_{i,j} v_i v_j \cos \theta_{ij}], i \in \mathcal{L}, \quad (18d)$$

where $\theta_{ij} := \theta_i - \theta_j$; $p_{l_i} := p_{l_i}(t)$ and $q_{l_i} := q_{l_i}(t)$ are respectively the real and reactive power demands at node i modeled as a time-varying constant-power load, i.e., p_{l_i} and q_{l_i} are not functions of v_i . The mapping \mathbf{h} in (1b) is given by concatenating (17) for $i \in \mathcal{G}$ and (18) for $i \in \mathcal{N}$. By defining $\mathbf{p}_{l_{\mathcal{G}}} = \{p_{l_i}\}_{i \in \mathcal{G}}$, $\mathbf{q}_{l_{\mathcal{G}}} = \{q_{l_i}\}_{i \in \mathcal{G}}$, $\mathbf{p}_{l_{\mathcal{L}}} = \{p_{l_i}\}_{i \in \mathcal{L}}$, $\mathbf{q}_{l_{\mathcal{L}}} = \{q_{l_i}\}_{i \in \mathcal{L}}$, the vector $\mathbf{d} = \{\mathbf{0}_{2G}, -\mathbf{p}_{l_{\mathcal{G}}}, -\mathbf{q}_{l_{\mathcal{G}}}, -\mathbf{p}_{l_{\mathcal{L}}}, -\mathbf{q}_{l_{\mathcal{L}}}\}$ is obtained.

C. Optimal power flow

The standard OPF problem typically only considers the algebraic variable \mathbf{a}^s and is given as

$$\min_{\mathbf{a}^s} c(\mathbf{a}^s) \quad \text{subj. to} \quad (18) \text{ and } \mathbf{a}^s \in \mathcal{A}. \quad (19)$$

If the cost function $c(\mathbf{z}^s)$ of the generalized OPF in (3) is only a function of algebraic variables \mathbf{a}^s , (3) can be solved by solving the standard OPF problem (19) to obtain the optimal \mathbf{a}^s . The variables \mathbf{x}^s and \mathbf{u}^s can then be found by plugging in \mathbf{a}^s in equations (17) and (16) while setting $\dot{\mathbf{x}} = \mathbf{0}$.

VII. NUMERICAL SIMULATIONS

This section provides a numerical assessment of the advantages of the LQR-OPF in comparison to a method where OPF and load-following control problems are treated separately. Prior to analyzing the case studies, the general simulation workflow of Fig. 2 is described.

The decoupled approach, one where OPF and stability are solved separately, is considered on the left-hand side of Fig. 2. Initially, the system is in steady-state and operates at \mathbf{z}^0 . For a forecasted load demand, $\mathbf{d}^s = \mathbf{d}^0 + \Delta \mathbf{d}^s$, the OPF (19) is solved yielding optimal steady-state setpoints \mathbf{a}^s , including generator real and reactive powers ($p_{g_i}^s, q_{g_i}^s$) and generator voltage magnitudes and phases (v_i^s, θ_i^s). For OPF, it holds that $\mathbf{a}^{\text{eq}} = \mathbf{a}^s$. The algebraic variables are then utilized to solve (16) upon setting $\dot{\mathbf{x}} = \mathbf{0}$ together with (17) to obtain steady-state setpoints of generator states \mathbf{x}^{eq} and control inputs \mathbf{u}^{eq} . The next steady-state equilibrium is then simply represented as $\mathbf{z}^{\text{eq}} = (\mathbf{x}^{\text{eq}}, \mathbf{a}^{\text{eq}}, \mathbf{u}^{\text{eq}})$. The DAEs (1a)–(1b), upon being subjected to the new load \mathbf{d}^s , depart from the initial equilibrium \mathbf{z}^0 . To steer the DAEs (1a)–(1b) to the next desired equilibrium point \mathbf{z}^{eq} , LQR is performed. Dynamic performance as well as costs of steady-state and load-following control are evaluated. The standard OPF (19) is solved using MATPOWER's `runopf.m`.

The proposed methodology is considered on the right-hand side of Fig. 2 where the OPF block is replaced by LQR-OPF (14) followed by a load-flow. LQR-OPF obtains optimal generator voltage setpoints $\{v_i^s\}_{i \in \mathcal{G}}$, real power setpoints $\{p_{g_i}^s\}_{i \in \mathcal{G} \setminus \{i_{\text{slack}}\}}$, and $\theta_{i_{\text{slack}}}^s$, while accounting for load-following costs that drive the DAEs (1a)–(1b) to the next desired equilibrium. These obtained setpoints are then input to a standard load-flow (performed by MATPOWER's `runpf.m`) by setting the following for $i \in \mathcal{G}$: $v_i^{\text{eq}} = v_i^s$, $p_{g_i}^{\text{eq}} = p_{g_i}^s$ for nonslack i , and $\theta_{i_{\text{slack}}}^{\text{eq}} = \theta_{i_{\text{slack}}}^s$. This process yields the remaining algebraic variables in \mathbf{a}^{eq} . Similar to the previous approach, the DAEs (16) and (17) are solved after setting $\dot{\mathbf{x}} = \mathbf{0}$ yielding optimal steady-state setpoints of states \mathbf{x}^{eq} and controls \mathbf{u}^{eq} . The next equilibrium is then given by $\mathbf{z}^{\text{eq}} = (\mathbf{x}^{\text{eq}}, \mathbf{a}^{\text{eq}}, \mathbf{u}^{\text{eq}})$. Once the DAE system departs from its initial equilibrium point \mathbf{z}^0 due to \mathbf{d}^s , LQR is applied to drive the system to the desired equilibrium \mathbf{z}^{eq} . LQR-OPF is solved using the CVX optimization toolbox [33]. Finally, a third approach where LQR-OPF in Fig. 2 is replaced by ALQR-OPF is considered. In Algorithm 1, the CARE is solved by MATLAB's `care.m` and the QP using CVX. Comparisons of the three approaches (OPF, LQR-OPF, and ALQR-OPF) are provided in Table I.

The workflow of Fig. 2 is applied to various networks as described in the next section. It is worth emphasizing that even though the derived control law required linearized system dynamics, all simulations are performed on the actual *nonlinear* dynamics and power flow equations, per the DAEs in (1a)–(1b). The dynamical system was modeled using MATLAB's `ode` suite. All computations use a personal computer with 32.0 GB RAM and 3.60 GHz CPU processor. MATLAB scripts that simulate the ensuing case studies are provided online [34].

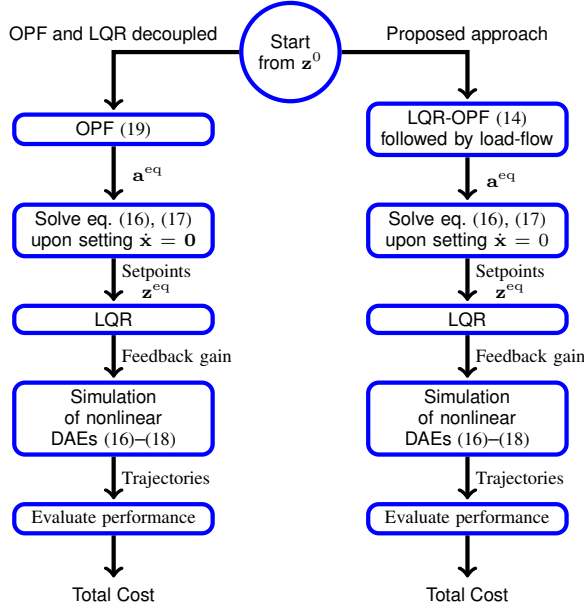


Fig. 2. Diagram showing the simulation steps.

A. Description of test networks

The workflow of Fig. 2 is applied to 9-, 14-, 39-, and 57-bus test networks as well as the 200-bus Illinois network. Steady-state data are obtained from the corresponding case files available in MATPOWER [35]. These data include bus admittance matrix \mathbf{Y} , steady-state real and reactive power demands, that is, $\mathbf{p}_l^0 := \{p_{l_G}^0, p_{l_C}^0\}$ and $\mathbf{q}_l^0 := \{q_{l_G}^0, q_{l_C}^0\}$, cost of real power generation $c(\mathbf{a}^s) = \sum_i c_2 (p_{g_i}^s)^2 + c_1 p_{g_i}^s + c_0$, as well as the limits of power generation and voltages in constraint (3d). Machine constants of (16a)–(16c) and (17) are taken from the PST toolbox, from case files `d3m9bm.m`, `d2asbegp.m`, and `datane.m`, respectively for the 9-, 14-, and 39-bus networks. For the 57- and the 200-bus networks, as well as the governor model of (16d) for all networks, based on ranges of values provided in PST [36], typical parameter values of $M_i = 0.2 \text{ pu} \times \text{sec}^2$, $D_i = 0 \text{ pu} \times \text{sec}$, $\tau_{d_i} = 5 \text{ sec}$, $x_{d_i} = 0.7 \text{ pu}$, $x_{q_i} = 0.5 \text{ pu}$, $x'_{d_i} = 0.07 \text{ pu}$, $\tau_{c_i} = 0.2 \text{ sec}$, and $R_i = 0.02 \frac{\text{Hz}}{\text{pu}}$ have been selected.

B. Regulation cost matrices \mathbf{Q} and \mathbf{R}

In accordance with (13), \mathbf{Q}^{-1} and \mathbf{R}^{-1} are selected to be diagonal with affine entries as follows

$$\mathbf{Q}_{\omega_i, \delta_i, m_i}^{-1} = \mathbf{R}_{r_i}^{-1} = \left(1 - \alpha \frac{p_{g_i}^s}{p_{g_i}^{\max}}\right), \quad (20a)$$

$$\mathbf{Q}_{e_i}^{-1} = \mathbf{R}_{f_i}^{-1} = \left(1 - \alpha \frac{q_{g_i}^s}{q_{g_i}^{\max}}\right), \quad (20b)$$

where $\mathbf{Q}_{\omega_i, \delta_i, m_i}$ refers to the diagonal entries of \mathbf{Q} corresponding to ω_i , δ_i , and m_i . Matrices \mathbf{Q}_{e_i} , \mathbf{R}_{r_i} , and \mathbf{R}_{f_i} are similarly defined. Parameter α is in the interval $[0, 1)$ that determines the amount of coupling between steady-state quantities and control costs through matrices \mathbf{Q} and \mathbf{R} . Quantities $p_{g_i}^{\max}$ and $q_{g_i}^{\max}$ are respectively the maximum real and reactive power limits of generator $i \in \mathcal{G}$.

The rationale behind choosing (20a) is that angle and frequency instability are usually remedied by generating real power. In this case, increase in steady-state real power generation $p_{g_i}^s$ leads to higher cost of frequency regulation. Similarly, the rationale behind choosing (20b) is that voltage stability is typically correlated with reactive power injection. This choice means that an increase in steady-state reactive power generation $q_{g_i}^s$ incurs a higher cost of voltage regulation.

C. Dynamical simulation with LQR

A step load increase of 10% in real power with power factor 0.9 is applied at $t = 0$. This implies that $\Delta p_{l_i}^s = 0.1 p_{l_i}^0$ and $\Delta q_{l_i}^s = 0.0484 q_{l_i}^0$, totaling to a load increase of $31.50 + j5.56 \text{ MVA}$ for the 9-bus system, $25.90 + j3.56 \text{ MVA}$ for the 14-bus system, $625.42 + j67.10 \text{ MVA}$ for the 39-bus system, $125.08 + j16.28 \text{ MVA}$ for the 57-bus, $222.87 + j30.74 \text{ MVA}$ for the 200-bus Illinois system. This load increase drives the nonlinear dynamics (1) out of the initial equilibrium. By applying LQR control according to the workflow in Fig. 2, the dynamics in (1) are steered to arrive at the desired equilibria obtained from the OPF and LQR-OPF.

With selections of $\alpha = 0.6$ and $T_{1qr} = 1000$, Table I lists the breakdown of steady-state, control, and total costs, as well as maximum frequency and voltage deviations from the optimal equilibrium of the LQR-OPF, ALQR-OPF with two iterations, and OPF. Column 3 gives the optimal objective of the LQR-OPF in (14) or the best objective found by the ALQR-OPF in Algorithm 1. Observe that the optimal objectives of LQR-OPF and ALQR-OPF are almost identical, which implies that the approximation in Algorithm 1 does not compromise optimality.

Steady-state costs in column 4 correspond to $c(\mathbf{a}^{\text{eq}})$ found by each approach. The LQR step in the diagram of Fig. 2 is solved using MATLAB's `care.m` by inputting $\mathbf{Q}(\mathbf{z}^{\text{eq}})$ and $\mathbf{R}(\mathbf{z}^{\text{eq}})$. This process yields \mathbf{P} and the corresponding feedback gain $\mathbf{K} = -\mathbf{R}^{-1} \mathbf{B}^T \mathbf{P}$. The estimates of the control costs are then calculated as $\frac{T_{1qr}}{2} (\mathbf{x}^{\text{eq}} - \mathbf{x}^0)^T \mathbf{P} (\mathbf{x}^{\text{eq}} - \mathbf{x}^0)^T$ and are given in column 5 of Table I. The total estimated costs are then the summation of steady-state and estimated control costs and are given in column 6. The computation times of LQR-OPF, ALQR-OPF, and OPF are listed in column 7. Notice that for the large 200-bus Illinois network, the LQR-OPF takes approximately 12 hours, while the ALQR-OPF solves the problem in less than three seconds and without significant loss in optimality.

Control costs reported in column 8 of Table I are computed as $\frac{T_{1qr}}{2} \int_0^{t_f} (\Delta \mathbf{x}'^T \mathbf{Q} \Delta \mathbf{x}' + \Delta \mathbf{u}'^T \mathbf{R} \Delta \mathbf{u}') dt$, that is, through numerical integration of the trajectories resulting from the simulation of the nonlinear DAEs. The total cost, given in column 9, is simply the summation of control and steady-state cost. Between the coupled and decoupled approaches, OPF exhibits lower steady-state cost but higher control cost. In terms of total cost, the LQR-OPF and ALQR-OPF show improved performance. The maximum frequency deviation is also much lower for LQR-OPF and ALQR-OPF than the OPF.

In Figs. 3 and 4 the dynamical performance of the 39-bus system under LQR-OPF, ALQR-OPF, and OPF in conjunction

TABLE I
COSTS COMPARISON BETWEEN LQR-OPF, ALQR-OPF, AND OPF METHODS AT $\alpha = 0.6$ UNDER LQR

Network	Method	Obj.	Steady-state cost (\$)	Control est. cost (\$)	Total est. cost (\$)	Comp. time (seconds)	Control cost (\$)	Total (\$)	Max. freq. dev. (Hz)	Max. volt. dev. (pu)
9-bus	LQR-OPF	6168.78	6144.11	26.30	6170.41	2.57	28.02	6172.13	0.0145	0.0262
	ALQR-OPF	6168.78	6144.25	26.16	6170.41	0.85	27.87	6172.11	0.0145	0.0261
	OPF	—	6113.60	329.02	6442.62	0.64	316.01	6429.61	0.0202	0.1240
14-bus	LQR-OPF	9209.27	9178.82	36.20	9215.01	2.32	36.95	9215.77	0.0052	0.0297
	ALQR-OPF	9209.28	9178.57	36.48	9215.04	0.74	37.26	9215.83	0.0053	0.0297
	OPF	—	9127.35	248.29	9375.64	0.26	248.13	9375.48	0.0120	0.0297
39-bus	LQR-OPF	55560.94	52872.28	2471.68	55343.95	18.95	3120.73	55993.51	0.0804	0.0820
	ALQR-OPF	55561.20	52871.80	2472.94	55344.74	1.39	3128.34	56000.14	0.0804	0.0816
	OPF	—	51386.02	12504.70	63890.72	0.23	13468.42	64854.44	0.1333	0.1157
57-bus	LQR-OPF	50169.04	48322.27	2468.43	50790.70	6.01	2306.30	50628.57	0.0602	0.0599
	ALQR-OPF	50177.06	48368.33	2410.75	50779.08	0.87	2260.24	50628.57	0.0593	0.0600
	OPF	—	47199.75	5829.34	53029.09	0.22	5889.98	53089.73	0.0944	0.0637
200-bus	LQR-OPF	52731.74	48347.04	4090.34	52437.38	44070.98	4089.44	52436.48	0.0283	0.0608
	ALQR-OPF	54575.99	50349.65	2424.85	52774.50	2.92	2526.84	52876.49	0.0199	0.0589
	OPF	—	48271.72	8724.08	56995.80	0.72	9258.04	57529.76	0.0468	0.0745

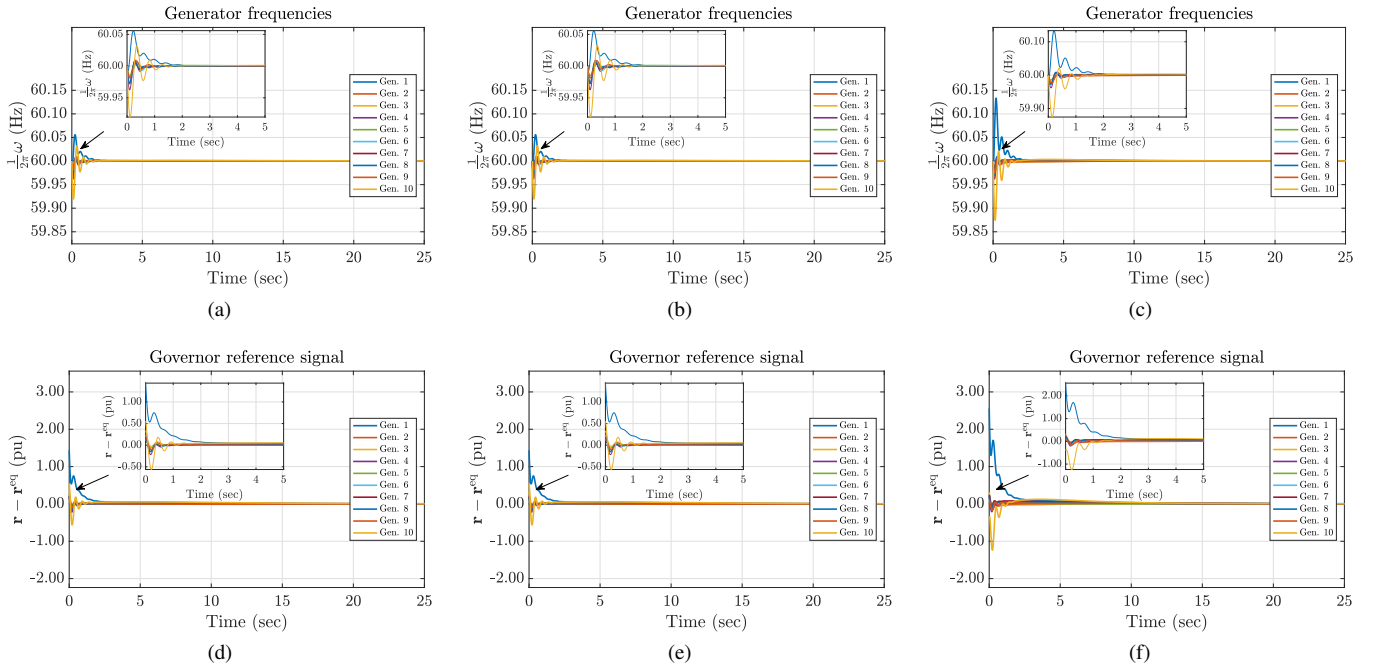


Fig. 3. Generator frequencies and governor signals using LQR-OPF (left), ALQR-OPF (center), and OPF (right).

with load-following LQR is depicted. Specifically, generator frequencies and governor reference signals are portrayed in Fig. 3 where it is observed that quantities, especially frequencies, resulting from OPF undergo higher fluctuations than those resulting from LQR-OPF and ALQR-OPF. In Fig. 4 the generator internal EMF, exciter field voltage, and nodal voltages are depicted. Notice that overall, voltages obtained from LQR-OPF and ALQR-OPF exhibit smaller deviations from the designated equilibria in comparison with those obtained from OPF. Deviations of generator angles δ also exhibit similar behavior. Plots for the remaining quantities (δ and \mathbf{m}) and the corresponding plots for the remaining test networks (including the 200-bus Illinois network) are available online [34].

D. Dynamical simulation with AGC

The LQR-OPF furnishes a steady-state operating point with desirable stability properties. After the steady-state operating point has been computed, one does not have to necessarily use LQR as a controller, but one could rather implement another dynamic control law such as AGC or PI-control [37], [38]. The purpose of this section is to examine the control cost to drive the system to the equilibrium computed by LQR-OPF or OPF when the control law is AGC.

To this end, the setup of Section VII-C is followed, but AGC is used to adjust the governor reference signal during the dynamical simulations instead of LQR. Dynamical equations describing the AGC for a multi-area power network are adopted from [37] and [38]. The selection of participation factors to steer the DAEs to the desired equilibrium follows

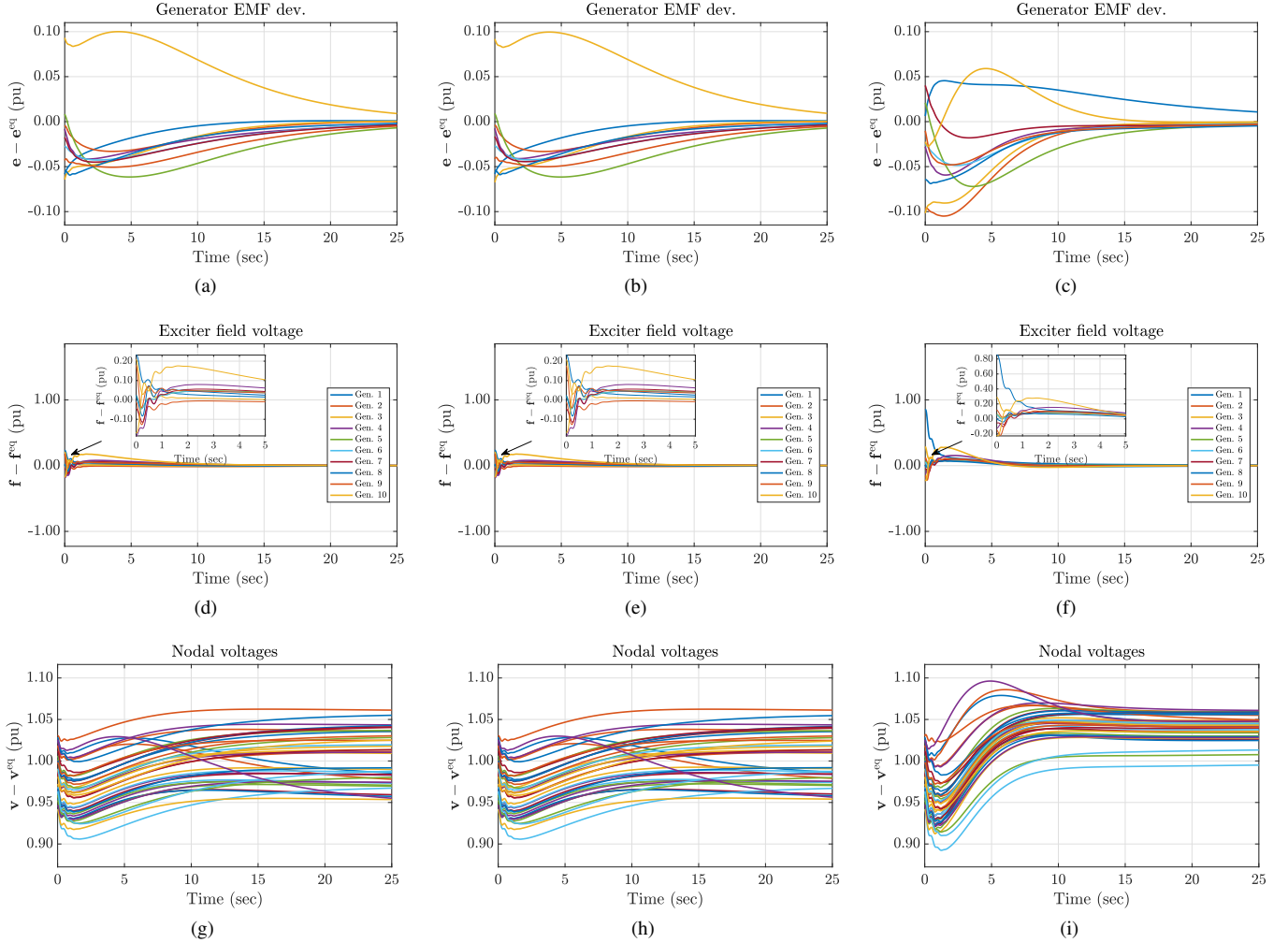


Fig. 4. Generator EMF, exciter voltage, and network nodal voltages using LQR-OPF (left), ALQR-OPF (center), and OPF (right).

the suggestions in [39, p. 87] for computer implementations. The specifics are detailed in the Appendix.

TABLE II
COSTS COMPARISON BETWEEN LQR-OPF, ALQR-OPF, AND OPF
METHODS AT $\alpha = 0.6$ UNDER AGC

Network	Method	Control cost (\$)	Total cost (\$)	Max. freq. dev. (Hz)	Max. volt. dev. (pu)
9-bus	LQR-OPF	35.92	6180.04	0.0144	0.0262
	ALQR-OPF	35.77	6180.02	0.0144	0.0261
	OPF	583.90	6697.50	0.0161	0.1240
14-bus	LQR-OPF	94.19	9273.01	0.0040	0.0297
	ALQR-OPF	94.30	9272.86	0.0041	0.0297
	OPF	590.84	9718.19	0.0096	0.0297
39-bus	LQR-OPF	4819.03	57691.30	0.0765	0.0782
	ALQR-OPF	4843.82	57715.62	0.0765	0.0772
	OPF	17781.72	69167.74	0.1321	0.1062
57-bus	LQR-OPF	4507.44	52829.71	0.0489	0.0599
	ALQR-OPF	4401.21	52769.55	0.0481	0.0600
	OPF	12652.76	59852.51	0.0760	0.0637
200-bus	LQR-OPF	9214.91	57561.95	0.0249	0.0608
	ALQR-OPF	5667.92	56017.57	0.0168	0.0589
	OPF	14959.59	63231.30	0.0358	0.0741

Table II reports the control and total costs of LQR-OPF and ALQR-OPF compared with OPF, when AGC is used

to adjust the governor signals r_i for $i \in \mathcal{G}$. Notice that the steady-state results are those previously given in Table I and only quantities pertaining to dynamical simulations have changed. It is observed that using AGC, setpoints provided by LQR-OPF and ALQR-OPF result in smaller control costs compared to OPF.¹ The corresponding dynamical performance for ALQR-OPF and OPF in conjunction with AGC is provided in Fig. 5–8. The setpoints provided by ALQR-OPF result in smaller frequency deviation and smaller ACE signal compared to the setpoints provided by OPF. The performance using the setpoints of LQR-OPF is similar to that of ALQR-OPF and has been omitted for brevity. Corresponding plots of other system quantities for the 39-bus network and the remaining test networks are also made available online [34].

E. Effect of coupling

Here, the effect of parameter α which couples steady-state variables to load-following control costs through (20) is studied. When the value of α increases to approach 1, entries of matrices \mathbf{Q} and \mathbf{R} increase as the values of $p_{g_i}^s$ and $q_{g_i}^s$

¹Table II indicates that total costs of ALQR-OPF are sometimes smaller than those of LQR-OPF. This happens because the optimality of LQR-OPF over ALQR-OPF is only guaranteed when the associated controller is LQR.

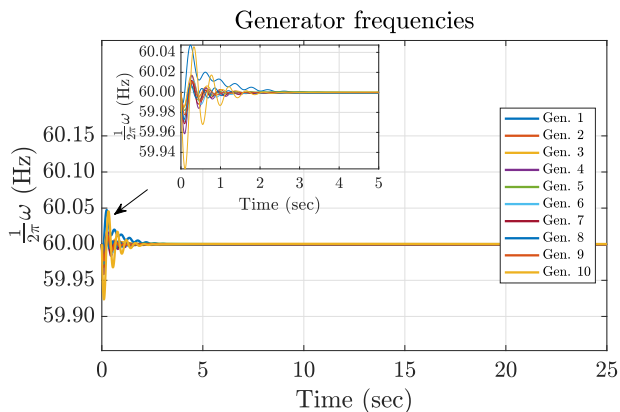


Fig. 5. Generator frequencies using ALQR-OPF in conjunction with AGC.

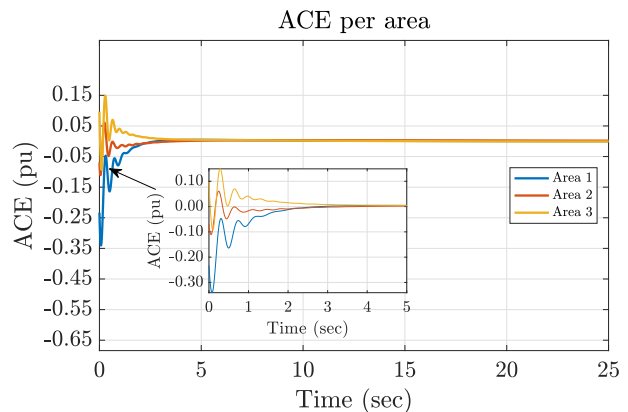


Fig. 7. Area control signal using ALQR-OPF in conjunction with AGC.

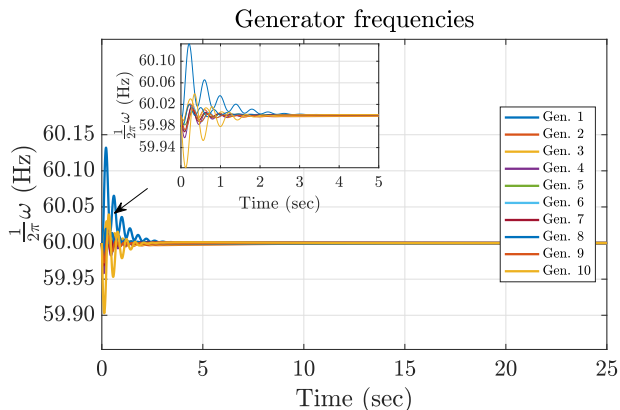


Fig. 6. Generator frequencies using OPF in conjunction with AGC.

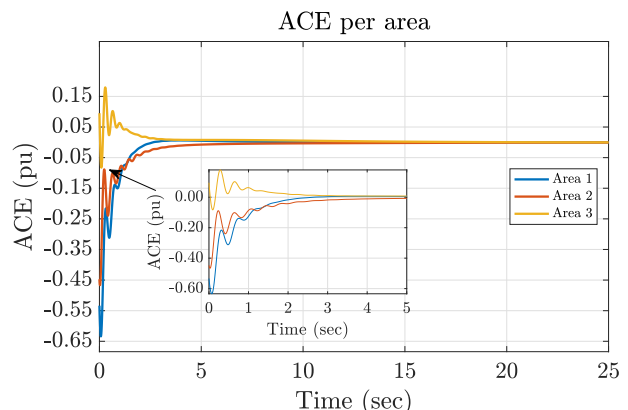


Fig. 8. Area control signal using OPF in conjunction with AGC.

approach their respective maximum. It is depicted in Fig. 9 that as the coupling coefficient α increases, control costs increase in both OPF and LQR-OPF. However, control costs of LQR-OPF are significantly lower than the costs incurred by the scheme where OPF and LQR are solved independently.

F. ALQR-OPF on larger networks

This section examines the performance of ALQR-OPF on larger networks. Table III lists the steady-state costs, estimated control costs (as computed by $\frac{T_{lqr}}{2}(\mathbf{x}^{eq} - \mathbf{x}^0)^\top \mathbf{P}(\mathbf{x}^{eq} - \mathbf{x}^0)$), total estimated costs, and computation times. The main observation is that ALQR-OPF yields significantly smaller total costs than OPF. The computation time of ALQR-OPF is larger than that of OPF, but it is worth noting that ALQR-OPF has been solved by a general-purpose solver, while MATPOWER's solver is specifically tailored to the OPF problem.

VIII. SUMMARY AND FUTURE WORK

An OPF framework is presented that in addition to solving for optimal steady-state setpoints provides an optimal feedback law to perform load-following control. The costs of load-following control is captured by a classical LQR control that accounts for deviations of system states and controls from their optimal steady-state setpoints. A joint formulation of OPF and load-following control, termed LQR-OPF, is obtained by combining a linearized OPF with an equivalent SDP formulation of

the LQR. Numerical tests verify that compared to a scheme where OPF and load-following control problems are solved separately, LQR-OPF features significantly improved dynamic performance and reduced overall system costs.

The proposed framework is general and allows for seamless incorporation of different power system applications, such as wind turbine and storage device dynamics—both operating at different time-scales. Recent work, for instance, demonstrates the impact of wind power injection on power system oscillations [40]. Future work includes integrating more modern applications into the proposed framework while investigating the regulation and cost benefits of this integration.

APPENDIX AGC IMPLEMENTATION

Denote by \mathcal{A} the set of areas of a power network and by \mathcal{A}_a the set of neighboring areas to area $a \in \mathcal{A}$. Further, denote respectively by $p_{aa'}$ and $p_{aa'}^{eq}$, the time-varying and equilibrium aggregate real power flows on the tie-lines from area $a \in \mathcal{A}$ into area $a' \in \mathcal{A}$. Notice that $p_{aa'}$ is a function of the voltage magnitudes and angles at the terminals of all the tie-lines connecting a to a' . The area control error (ACE) for area $a \in \mathcal{A}$ is then computed as

$$ACE_a = \sum_{a' \in \mathcal{A}_a} (p_{aa'} - p_{aa'}^{eq}) + b_a \left(\frac{1}{|G_a|} \sum_{i \in G_a} \omega_i - \omega^s \right) \quad (21)$$

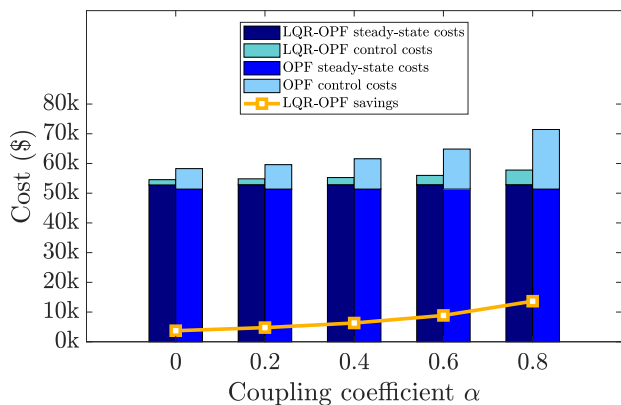


Fig. 9. Effect of coupling between steady-state variables and control cost matrices \mathbf{Q} and \mathbf{R} . As coupling coefficient α increases, LQR-OPF results in more savings than the decoupled OPF and LQR approach.

TABLE III
ALQR-OPF ON LARGER NETWORKS

Network	Method	Steady-state cost (\$)	Control est. cost (\$)	Total est. cost (\$)	Comp. time (seconds)
1354-bus	ALQR-OPF	82612	2311022	2393635	72.65
	OPF	81688	8279013	8360702	6.06
2383-bus	ALQR-OPF	2235711	21174	2256885	325.72
	OPF	2217287	123999	2341287	9.86
2869-bus	ALQR-OPF	149453	3255044	3404498	683.74
	OPF	147865	14830044	14977910	52.70

where \mathcal{G}_a denotes the set of generators in area a , and $b_a = \sum_{i \in \mathcal{G}_a} (\frac{1}{R_i} + D_i)$ is the area bias factor.

AGC uses the ACE signal to provide a command to the governor reference signal. The corresponding dynamical equations for area $a \in \mathcal{A}$ are

$$\dot{y}_a = K_a \left(-y_a - ACE_a + \sum_{i \in \mathcal{G}_a} p_{g_i}^{eq} \right) \quad (22a)$$

$$r_i = K_i y_a, \quad i \in \mathcal{G}_a, \quad (22b)$$

where K_a is an integrator gain, K_i is the participation factors of generator i , and r_i is fed back into (16d). The participation factors are set to $K_i = p_{g_i}^{eq} / \sum_{i \in \mathcal{G}_a} p_{g_i}^{eq}$ so that the power network will be steered to the desired equilibrium. Notice that the sum of participation factors per area equals unity.

REFERENCES

- [1] A. Gomez-Exposito, A. J. Conejo, and C. Canizares, *Electric Energy Systems: Analysis and Operation*. CRC Press, 2009.
- [2] F. Galiana, F. Bouffard, J. Arroyo, and J. Restrepo, "Scheduling and Pricing of Coupled Energy and Primary, Secondary, and Tertiary Reserves," *Proc. IEEE*, vol. 93, no. 11, pp. 1970–1983, Nov. 2005.
- [3] M. Andreasson, D. V. Dimarogonas, H. Sandberg, and K. H. Johansson, "Distributed control of networked dynamical systems: Static feedback, integral action and consensus," *IEEE Trans. Autom. Control*, vol. 59, no. 7, pp. 1750–1764, July 2014.
- [4] Q. Shafiee, J. M. Guerrero, and J. C. Vasquez, "Distributed secondary control for islanded microgrids—A novel approach," *IEEE Trans. Power Electron.*, vol. 29, no. 2, pp. 1018–1031, Feb. 2014.
- [5] F. Dörfler, J. W. Simpson-Porco, and F. Bullo, "Breaking the hierarchy: Distributed control and economic optimality in microgrids," *IEEE Trans. Control Netw. Syst.*, vol. 3, no. 3, pp. 241–253, Sept. 2016.
- [6] F. Dörfler and S. Grammatico, "Gather-and-broadcast frequency control in power systems," *Automatica*, vol. 79, pp. 296–305, 2017.

- [7] C. Zhao, U. Topcu, N. Li, and S. Low, "Design and stability of load-side primary frequency control in power systems," *IEEE Trans. Autom. Control*, vol. 59, no. 5, pp. 1177–1189, May 2014.
- [8] N. Li, C. Zhao, and L. Chen, "Connecting automatic generation control and economic dispatch from an optimization view," *IEEE Trans. Control Netw. Syst.*, vol. 3, no. 3, pp. 254–264, Sept. 2016.
- [9] X. Zhang and A. Papachristodoulou, "A real-time control framework for smart power networks: Design methodology and stability," *Automatica*, vol. 58, pp. 43–50, 2015.
- [10] E. Mallada, C. Zhao, and S. Low, "Optimal load-side control for frequency regulation in smart grids," *IEEE Trans. Autom. Control*, to be published.
- [11] D. Gan, R. J. Thomas, and R. D. Zimmerman, "Stability-constrained optimal power flow," *IEEE Trans. Power Syst.*, vol. 15, no. 2, pp. 535–540, May 2000.
- [12] L. Tang and W. Sun, "An automated transient stability constrained optimal power flow based on trajectory sensitivity analysis," *IEEE Trans. Power Syst.*, vol. 32, no. 1, pp. 590–599, Jan. 2016.
- [13] Y. Xu, J. Ma, Z. Y. Dong, and D. J. Hill, "Robust transient stability-constrained optimal power flow with uncertain dynamic loads," *IEEE Trans. Smart Grid*, vol. 8, no. 4, pp. 1911–1921, 2017.
- [14] Y. Xu, M. Yin, Z. Dong, R. Zhang, D. J. Hill, and Y. Zhang, "Robust Dispatch of High Wind Power-Penetrated Power Systems against Transient Instability," *IEEE Trans. Power Syst.*, to be published.
- [15] X. Xu, H. Zhang, C. Li, Y. Liu, W. Li, and V. Terzija, "Optimization of the Event-Driven Emergency Load-Shedding Considering Transient Security and Stability Constraints," *IEEE Trans. Power Syst.*, vol. 32, no. 4, pp. 2581–2592, July 2017.
- [16] R. Zarate-Minano, F. Milano, and A. J. Conejo, "An OPF methodology to ensure small-signal stability," *IEEE Trans. Power Syst.*, vol. 26, no. 3, pp. 1050–1061, Aug. 2011.
- [17] P. Li, J. Qi, J. Wang, H. Wei, X. Bai, and F. Qiu, "An SQP method combined with gradient sampling for small-signal stability constrained opf," *IEEE Trans. Power Syst.*, vol. 32, no. 3, pp. 2372–2381, May 2017.
- [18] E. Mallada and A. Tang, "Dynamics-aware optimal power flow," in *Proc. 52nd IEEE Conf. Decision and Control*, Florence, Italy, Dec. 2013, pp. 1646–1652.
- [19] P. Li, H. Wei, B. Li, and Y. Yang, "Eigenvalue-optimisation-based optimal power flow with small-signal stability constraints," *IET Generation, Transmission & Distribution*, vol. 7, no. 5, pp. 440–450, May 2013.
- [20] C. E. Fosha and O. I. Elgerd, "The megawatt-frequency control problem: A new approach via optimal control theory," *IEEE Trans. Power App. Syst.*, vol. 89, no. 4, pp. 563–577, Apr. 1970.
- [21] A. K. Singh and B. C. Pal, "Decentralized control of oscillatory dynamics in power systems using an extended LQR," *IEEE Trans. Power Syst.*, vol. 31, no. 3, pp. 1715–1728, May 2016.
- [22] J. A. Taylor, A. Nayyar, D. S. Callaway, and K. Poolla, "Consolidated dynamic pricing of power system regulation," *IEEE Trans. Power Syst.*, vol. 28, no. 4, pp. 4692–4700, Nov. 2013.
- [23] I. Hiskens and M. Pai, "Power system applications of trajectory sensitivities," in *Proc. Power Engineering Society Winter Meeting*, vol. 2, New York, NY, USA, Jan. 2002, pp. 1200–1205.
- [24] L. Tang and J. McCalley, "Trajectory sensitivities: Applications in power systems and estimation accuracy refinement," in *Proc. Power & Energy Society General Meeting*, Vancouver, BC, Canada, July 2013, pp. 1–5.
- [25] D. K. Molzahn, "Incorporating squirrel-cage induction machine models in convex relaxations of OPF problems," *IEEE Trans. Power Syst.*, to be published.
- [26] S. Boyd, L. E. Ghaoui, E. Feron, and V. Balakrishnan, *Linear Matrix Inequalities in Systems and Control Theory*. SIAM, 1994, vol. 15.
- [27] Y. Cui and R. Kavasseri, "A particle filter for dynamic state estimation in multi-machine systems with detailed models," *IEEE Trans. Power Syst.*, vol. 30, no. 6, pp. 3377–3385, Nov. 2015.
- [28] G. Valverde and V. Terzija, "Unscented Kalman filter for power system dynamic state estimation," *IET Generation, Transmission & Distribution*, vol. 5, no. 1, pp. 29–37, Jan. 2011.
- [29] A. F. Taha, J. Qi, J. Wang, and J. H. Panchal, "Risk mitigation for dynamic state estimation against cyber attacks and unknown inputs," *IEEE Trans. Smart Grid*, to be published.
- [30] R. Madani, S. Sojoudi, and J. Lavaei, "Convex Relaxation for Optimal Power Flow Problem: Mesh Networks," *IEEE Trans. Power Syst.*, vol. 30, no. 1, pp. 199–211, Jan. 2015.
- [31] V. Balakrishnan and L. Vandenberghe, "Semidefinite programming duality and linear time-invariant systems," *IEEE Trans. Autom. Control*, vol. 48, no. 1, pp. 30–41, Jan. 2003.

- [32] G. B. Giannakis, V. Kekatos, N. Gatsis, S. J. Kim, H. Zhu, and B. F. Wollenberg, "Monitoring and optimization for power grids: A signal processing perspective," *IEEE Signal Process. Mag.*, vol. 30, no. 5, pp. 107–128, Sept. 2013.
- [33] M. Grant and S. Boyd, "CVX: Matlab software for disciplined convex programming, version 2.1," <http://cvxr.com/cvx>, Mar. 2014.
- [34] M. Bazrafshan, "LQR-OPF," 2017. [Online]. Available: <https://github.com/hafezbazrafshan/LQR-OPF>
- [35] R. D. Zimmerman, C. E. Murillo-Sanchez, and R. J. Thomas, "Matpower: Steady-state operations, planning, and analysis tools for power systems research and education," *IEEE Trans. Power Syst.*, vol. 26, no. 1, pp. 12–19, Feb. 2011.
- [36] J. H. Chow and K. W. Cheung, "A toolbox for power system dynamics and control engineering education and research," *IEEE Trans. Power Syst.*, vol. 7, no. 4, pp. 1559–1564, Nov. 1992.
- [37] J. Zhang and A. Dominguez-Garcia, "On the Impact of Measurement Errors on Power System Automatic Generation Control," *IEEE Trans. Smart Grid*, to be published.
- [38] J. D. Glover, M. S. Sarma, and T. J. Overbye, *Power System Analysis and Design*, 5th ed. Cengage Learning, 2012.
- [39] A. J. Wood and B. F. Wollenberg, *Power Generation, Operation, and Control*, 3rd ed. John Wiley & Sons, 2012.
- [40] S. Chandra, D. F. Gayme, and A. Chakraborty, "Time-scale modeling of wind-integrated power systems," *IEEE Trans. Power Syst.*, vol. 31, no. 6, pp. 4712–4721, Nov. 2016.